JOURNAL OF Materials CHEMISTRY

Growth of GaSb whiskers by thermal decomposition of a single source precursor

Andreas Kuczkowski, Stephan Schulz* and Wilfried Assenmacher

Institut für Anorganische Chemie der Universität Bonn, Gerhard-Domagk-Str. 1, D-53121 Bonn, Germany. E-mail: sschulz@uni-bonn.de

Received 30th May 2001, Accepted 2nd August 2001
First published as an Advance Article on the web 9th October 2001

Thermal decomposition reactions of the Lewis acid–base adducts *t*-Bu_3Ga–Sb(*t*-Bu)$_3$ **1** and *t*-Bu_3Ga–Sb(*i*-Pr)$_3$ **2** were investigated at different temperatures. Both adducts lead to the formation of crystalline GaSb particles in the temperature range of 275–450 °C, proving their potential to serve as single source precursors for the preparation of GaSb. In contrast to **1**, **2** tends to form crystalline, highly-oriented GaSb whiskers under the pyrolysis conditions. Detailed temperature-dependent studies clearly reveal the strong influence of the decomposition conditions on the whisker growth. While at temperatures between 275 and 375 °C single GaSb needles preferably were formed, higher temperatures (400–450 °C) lead to the formation of crystalline GaSb dendrites. As-prepared carbon-free, cubic GaSb whiskers were characterized in detail by SEM, TEM, electron diffraction, EDX and EEL spectroscopy.

Introduction

Group 13 antimonides are narrow direct band gap semiconductors with small band gaps (E_g [eV]: 1.60 (AlSb), 0.67 (GaSb), 0.16 eV (InSb)) and high electron mobility, which render them very attractive for potential applications in optoelectronic devices. GaSb for instance is used for the production of light-emitting and light-detecting devices operating in the 2 μm wavelength range[1] as well as in field effect transistors,[2] infrared detectors[3] and hot electron transistors.[4] Traditionally, it has been prepared by MBE (molecular beam epitaxy)[5] and LPE (liquid phase epitaxy)[6] processes. The CVD process, which has become the most important technological process for the preparation of thin films of binary group 13 nitrides, phosphides and arsenides (ME; M = Al, Ga, Sb) since initial studies by Manasevit almost 40 years ago,[7] surprisingly is less important for the synthesis of the corresponding antimonides.[8] So far, only GaSb and InSb films were obtained by CVD processes,[9] while the preparation of AlSb films of reasonable quality failed.[10] To the best of our knowledge, all AlSb films obtained by this technology show unacceptably large concentrations (impurities) of carbon.

The growth of thin films of binary group 13 nitrides, phosphides and arsenides by CVD typically uses group 13 trimethyl derivatives MMe_3 (M = Al, Ga, In) and group 15 hydrides EH_3. The latter, which produce atomic hydrogen during the CVD process, are used in great excess to reduce any carbon contamination of the resulting materials. However, an analogous process is not possible for the preparation of group 15 antimonides due to the following reasons:

(1) SbH_3, formally an ideal precursor,[11] can't be used for an industrial process because it is thermally very unstable and decomposes even at temperatures below −60 °C. Similar problems are valid for primary and secondary stibines of the type $RSbH_2$ and R_2SbH, in particular those with small substituents (R = Me, Et).

(2) The presence of an excess of the stibine during film growth, which may lead to the formation of elemental Sb on the substrate, has to be strictly avoided because under typical growth conditions, the volatility of elemental Sb is very low. This is in sharp contrast to the lighter group 15 elements, N, P and As. The very low volatility of elemental Sb prevents it from getting removed from the surface. To obtain the desired binary material, an almost equimolar molar ratio of the group 13 precursor and the stibine is necessary.

For these reasons, group 13 trialkyls R_3M (M = Al, Ga, In) and triorganostibines R_3Sb typically serve as precursors.[12] However, both the inability to produce atomic hydrogen during the pyrolysis as well as the very stable metal–carbon bonds favor the incorporation of large amounts of C into the resulting material. In the case of the growth of GaSb and InSb, these problems have almost been solved by using $Sb(NMe_2)_3$,[13] which contains weaker Sb–N bonds, but this particular precursor failed for the synthesis of AlSb.

A possible alternative pathway to overcome the described problems during the growth of binary group 13 antimonides is based on a different concept, the *single source precursor concept*. A single source precursor contains the specific elements of the desired material connected by a chemical bond pre-formed in a single molecule. Typically Lewis acid–base adducts R_3M–ER'_3 or heterocycles of the type $[R_2MER'_2]_x$ are used. Their most striking properties are their lower metal–carbon bond energies compared to the pure group 13 and group 15 trialkyls, allowing lower pyrolysis temperatures, their reduced air- and moisture-sensitivity and their reduced toxicity. However, they typically have much lower volatilities. So far, reports on the preparation of binary group 13 antimonides by thermal decomposition of single source precursors are very rare. Only $[Me_2MSb(t\text{-}Bu)_2]_3$ (M = Ga, In) and $[R_2AlSb(SiMe_3)_2]_2$ (R = Et, *i*-Bu) have been reported to yield crystalline MSb films by CVD processes.[14] The small number of reports clearly results from the under-explored precursor chemistry. Standard metal organic reactions like H_2-, alkane- or salt-elimination reactions, which have been developed for the synthesis of ME heterocycles containing the lighter elements of group 15, are not useful synthetic pathways for the synthesis of group 13–Sb heterocycles. In addition, Lewis acid–base adducts containing trialkylstibines are much less stable compared to the corresponding amine and phosphine adducts due to the reduced Lewis basicity of the stibines. Therefore, compounds of the desired types were almost unknown,[14a,15] until we[16] and others[17] started only five years ago detailed investigations on the synthesis of simple Lewis acid–base adducts R_3M–SbR'_3 and heterocycles $[R_2MSbR'_2]_x$ (M = Al,

Ga, In; R, R′ = alkyl, $SiMe_3$). Furthermore, Wells *et al.* also proved adducts and heterocycles bearing silyl substituents to be suitable precursors for the synthesis of GaSb nano-particles by simple thermal decomposition reactions.[17]

However, we focused on the synthesis of completely alkyl-substituted adducts to eliminate the possibility of any Si contamination of the resulting material. In particular adducts containing weak Ga–C and Sb–C bonds appeared attractive for initial studies. Therefore, *i*-Pr and *t*-Bu substituted adducts were chosen for preliminary decomposition studies, because the M–C bond energies for Sb–(*i*-Pr) and Sb–(*t*-Bu) bonds are much lower than for Sb–Me or Sb–Et bonds.[18] In addition, secondary and tertiary ligands offer the possibility for a β-hydride elimination pathway, which is known to produce materials of good quality containing very low C impurities. The results of our investigations are described herein.

Experimental

General sample preparation

15 mg of the particular adduct was placed under an Ar atmosphere in a glass tube, which was then sealed under atmospheric pressure. The tube was heated with a heating rate of 50 °C h^{-1} to the desired temperature. Heating was maintained for 2 h at this specific temperature, followed by cooling to ambient temperature with a cooling rate of 100 °C h^{-1}. In all cases, the resulting tube was covered inside with a dark grey, shiny film.

Sample characterization

The material was characterized by means of electron microscopy. Scanning electron microscopy studies (SEM) were carried out on a Philips XL20 (W filament), equipped with an energy dispersive X-ray spectroscopy (EDX) device (Noran Voyager, Si(Li)). Pieces of the broken glass tube covered with the GaSb material were sputtered with a thin gold film to improve the conductivity and therefore the contrast of the material film.

Transmission electron microscopy studies (TEM) were performed either on a Philips CM30ST (LaB_6 cathode) at 300 keV equipped with a parallel electron energy loss (EEL) spectrometer (Gatan P666) or on a Philips CM300UT (FEG) at 297 keV equipped with a SlowScan CCD (Gatan, 2k × 2k) and an imaging filter (Gatan GIF) for recording EEL spectra and energy-filtered images with a second CCD (1k × 1k) at the end of the filter. A HP–Ge EDX detector (Noran Voyager) was present on both transmission electron microscopes for EDX analysis. Sb-L and Ga-K lines were used for quantification of the EDX data. The Sb/Ga ratio was determined using the "Metal-Thin-Foil-Method" with *k*-factors (Cliff–Lorrimer method) yielded from calibration of the EDX system with certified GaSb from Aldrich Chemical Company. The samples were prepared on perforated carbon foils without further grinding.

Results and discussion

t-Bu_3Ga–Sb(*t*-Bu)$_3$ (1)

Adduct **1** was pyrolysed in the described manner at temperatures between 250 and 450 °C. The morphology of the resulting films as determined by SEM is very uniform and the crystal size is not influenced by the temperature of pyrolysis. A typical image of a sample obtained at 400 °C is seen in Fig. 1.

The material is crystalline, with particles of 500–1000 nm length. The bigger particles with bright contrast are glass fragments from breaking the tube. Due to their reduced

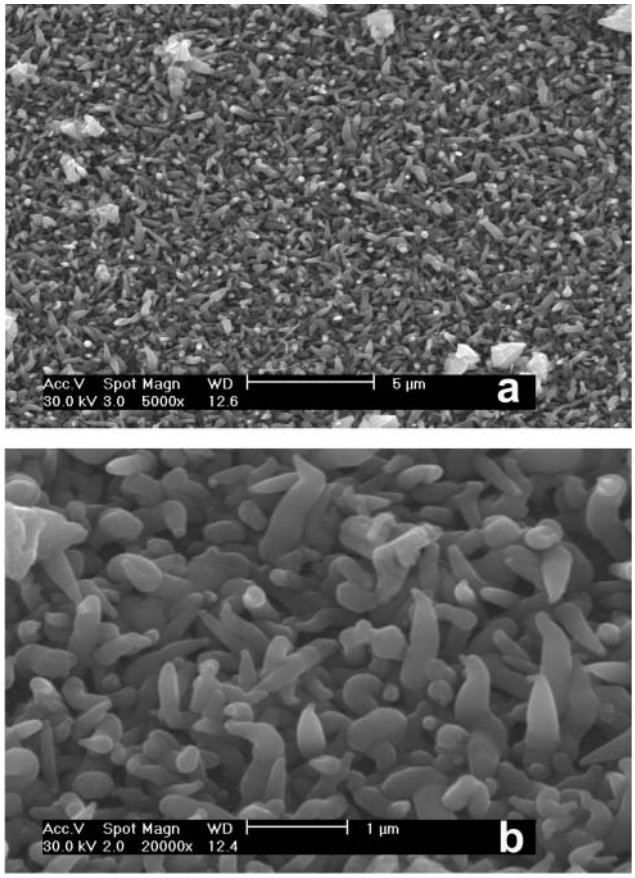

Fig. 1 SEM images of GaSb crystallites obtained from *t*-Bu_3Ga–Sb(*t*-Bu)$_3$ **1** at 400 °C.

conductivity, they appear as white particles. EDX studies both of single crystallites and bigger areas show the presence of Ga and Sb in an atomic ratio of 1.00–1.04, indicating the formation of slightly Ga-rich particles.[19] In addition, the spectra obtained from bigger areas show the presence of Si (1–2%), which is probably due to the glass substrate.

To investigate the morphology, crystallinity and elemental composition of the particles in more detail, TEM studies were performed. Typical bright-field images of particles as obtained from precursor **1** at 400 °C are shown in Fig. 2.

The particle size ranges from 200 to 500 nm in length, which is in agreement with results obtained by SEM. Unfortunately, only a few crystals are thin enough to be electron-transparent. However, they appear to be built up by several layers of crystalline plates. EDX studies performed on single particles reveal the results as obtained by SEM. The crystals contain an almost ideal 1 : 1 composition of Ga and Sb, while Si could not be detected. The element distribution within the particles is uniform. The slight Ga excess is unsurprising since CVD experiments, *e.g.* for the preparation of GaAs or InP, often lead to group 13 element-rich materials. The quantification of the EDX analyses as obtained from measurements on different particles is shown in Table 1.

EEL spectroscopy was used to determine any impurities such as C and O within the crystalline particles. While the carbon concentration in any particle analyzed is below the detection limit of EELS, O was clearly present within the samples. However, the exact concentration couldn't be quantified accurately since the O-K line (532 eV) is very close to the Sb-M line (540 eV).[20] However, the amount of oxygen does not increase with the crystal thickness, indicating oxygen to be present as a surface layer. Contamination of the GaSb particles with O is reliable due to the sensitivity of GaSb towards surface oxidation. Since the sample preparation

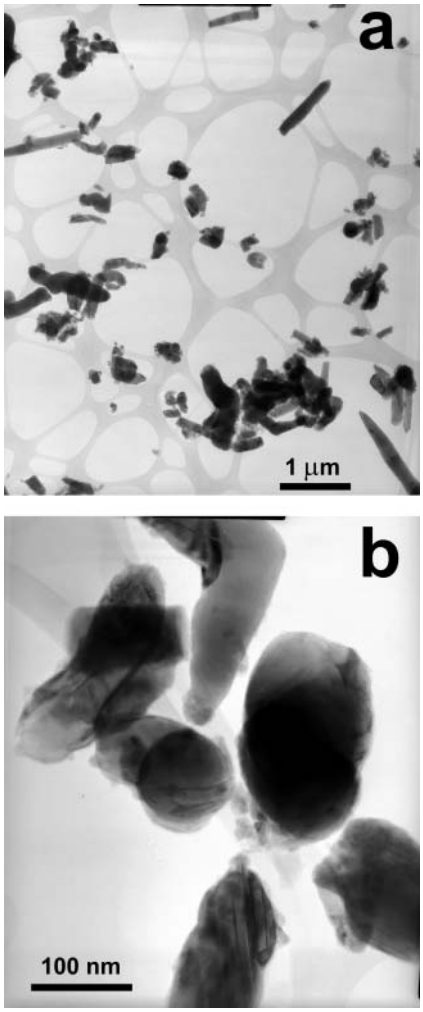

Fig. 2 TEM bright-field images at different magnifications of GaSb obtained from **1** at 400 °C.

wasn't performed under an inert gas atmosphere, such a process is possible.

The particles were also investigated by selected-area electron diffraction. The well-defined, sharp diffraction patterns of the GaSb nanoparticles clearly proved the particles to be crystalline. They show Debye–Scherrer rings with *d*-spacings comparing well to literature values of sphalerite-type, cubic GaSb. Particles obtained at lower (375–275 °C) and higher temperatures (450 °C) showed comparable results, which are therefore not presented in detail herein.

The results obtained from precursor **1** clearly demonstrate its potential to serve as a single source precursor for the growth of crystalline GaSb films. In particular the absence of any carbon contamination and the very low decomposition temperatures render **1** very attractive for further, detailed MOCVD studies. These are currently under investigation.

t-Bu_3Ga–Sb(*i*-Pr)$_3$ (2)

The pyrolysis experiments and the sample preparation of adduct **2** were performed in the same way as described for compound **1**. However, the surface morphology of the films as obtained from precursor **2** is clearly different from that of **1**. Fig. 3 shows images of a film obtained at 400 °C.

Table 1 Quantification of EDX analyses as obtained from different particles

	1	2	3	4	5
Ga	50.7	50.3	50.1	50.9	50.4
Sb	49.3	49.7	49.9	49.1	49.6
Ga : Sb	1.03	1.01	1.00	1.04	1.02

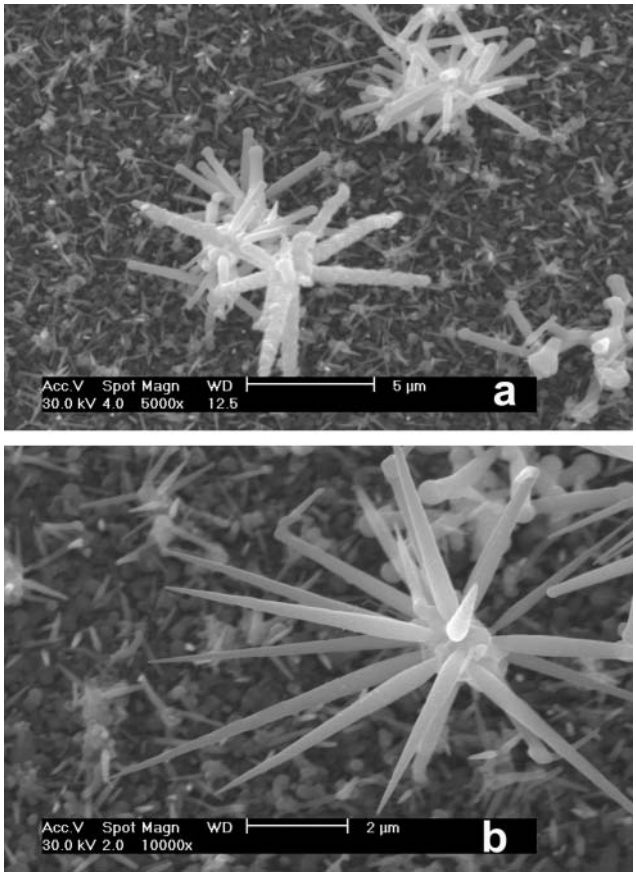

Fig. 3 SEM images of GaSb crystallites obtained from *t*-Bu_3Ga–Sb(*i*-Pr)$_3$ **2** at 400 °C.

The sample contains particles of 500–1000 nm in length, comparable to those obtained from precursor **1**. These crystallites are GaSb, as was demonstrated by TEM and EDX studies.[21] In addition, particles of clearly different shape are present. Large needles (up to 5 μm), which seem to be grown from a common ball-shaped origin, with large length/diameter ratios, as well as single needles were detected. EDX spectra obtained from the dendritic-type particles in the scanning electron microscope indicate the formation of a Ga-rich material. However, the results differ significantly in respect to the Ga : Sb molar ratio, which varies from 1.70 to 2.20. To avoid any effect from material beneath the needles and to quantify the exact Ga : Sb molar ratio of these particles, TEM studies were performed. The dendrites were mechanically separated from the films using a light microscope and placed on a carbon foil supported by a Cu grid. Fig. 4 shows bright-field images at different magnifications of as-prepared dendrites.

Both the single needles as well as a complete dendrite, containing a ball-shaped center, from which several single needles are grown in different directions, can clearly be seen. Since the preparation technique prevents any powdering, polishing or etching of the material, only some dendrites are electron transparent. Each needle is capped by a spherule. EDX studies (Fig. 5) performed on several individual centers, needles and ball-shaped tips showed different Ga : Sb molar ratios, as is summarized in Table 2.

Quantification of several EDX analyses of the dendrite centers indicate a 2 : 1 stoichiometry (Ga : Sb). However, electron diffraction studies only reveal the presence of cubic-type GaSb. In addition, the electron diffraction patterns show a strong and diffuse background beside the Bragg intensities. Obviously, the centers contain a variable excess of amorphous

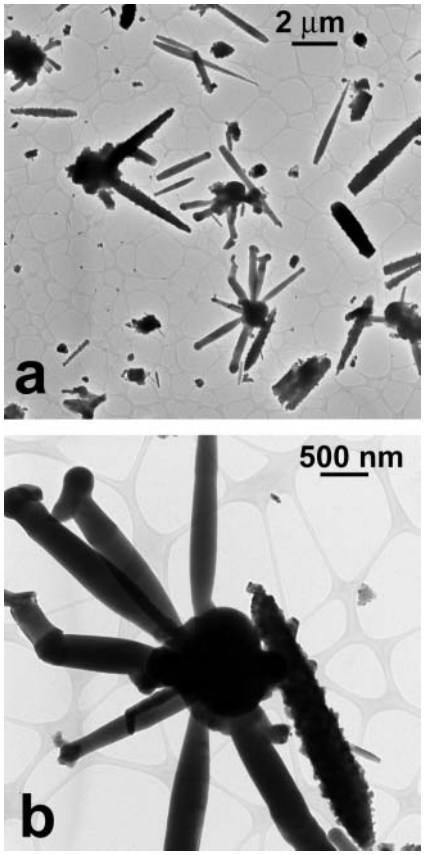

Fig. 4 TEM bright-field images at different magnifications of dendrites obtained from **2** at 400 °C.

Ga. In contrast to these results, the Ga : Sb molar ratio within the single needles is almost equal to 1.

To determine the concenrations of C and O within the particles, EEL spectra were recorded. A typical spectrum of a single crystalline needle is shown in Fig. 6. The intensity of inelastic scattered electrons is spread at three different amplifications, due to its large decrease over the given energy range.

Ga and Sb have ionization edges at $\Delta E = 1120$ eV (Ga L) and

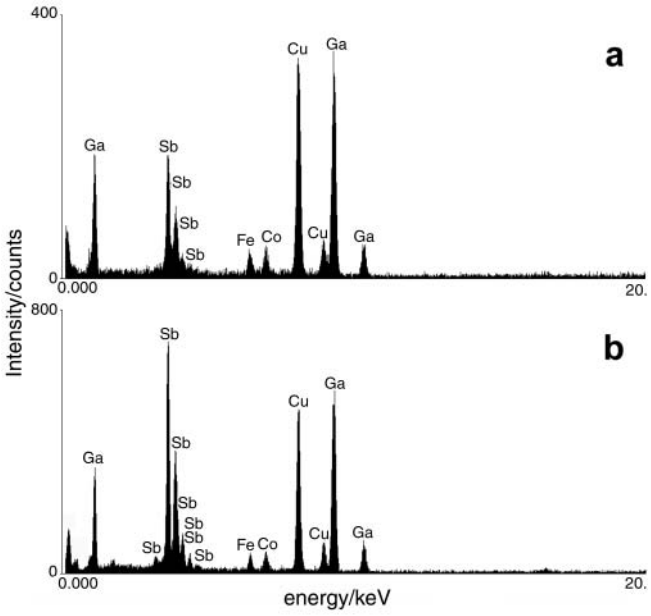

Fig. 5 EDX spectra obtained at a ball-shaped dendrite center (a) and at a single needle (b). Additional elements in the EDX spectra are caused by the copper grid (Cu) supporting the sample and by the pole piece of the microscope (Fe, Co), as was shown by a blank test.

Table 2 Quantification of EDX analyses as obtained at different centers, needles and tips

	Center				Needle				Tip	
	1	2	3	4	1	2	3	4	1	2
Ga	63.7	66.5	65.6	68.7	50.8	51.2	50.1	50.3	99.8	99.7
Sb	36.3	33.5	34.4	31.3	49.2	48.8	49.9	49.7	0.2	0.3
Ga : Sb	1.75	1.98	1.91	2.19	1.03	1.05	1.00	1.02	—	—

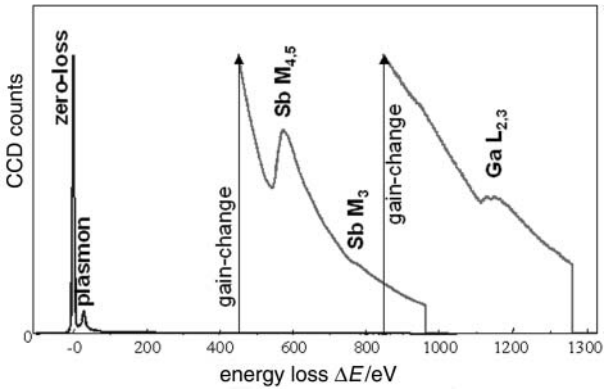

Fig. 6 EEL spectra of a single crystalline GaSb needle in the range from 0 to 1300 eV energy loss.

$\Delta E = 540$ eV (Sb M). In addition, O was found as a very small shoulder at $\Delta E = 532$ eV (O K) close to the Sb M-edge. C, showing a sharp edge at $\Delta E = 283$ eV (C K), could not be detected within the samples, even after background correction and deconvolution against plural scattering. The Ga : Sb molar ratio within the needles is uniform, varying only from 1.00 to 1.03. In contrast to the results obtained for the center and the needles, the tips contain almost pure, amorphous Ga. This is visualized in the Sb-distribution map as obtained from a single needle.

The Sb-distribution map was calculated by means of energy-filtered imaging, which was recorded at the tip of the needle. An intensity profile of the Sb distribution was calculated for the area indicated by the box in Fig. 7.[22] The homogeneous distribution of Sb within the crystalline needle can clearly be seen. In contrast, the amorphous tip contains almost no Sb. However, the drop of the Sb-concentration curve is not abrupt, indicating the tip to be partially grown into the needle. The needle is covered by a small amorphous, O-containing layer, resulting from a surface oxidation process.

Some needles are thin enough to be electron transparent, so they were subsequently investigated. The needles were found to be very often macled, as can be seen in Fig. 8. Twinning is also observed for small areas.

As was found for precursor **1**, SA (selected area) electron diffraction patterns of the nanoparticles show Debye–Scherrer rings with *d*-spacings comparing well to literature values of sphalerite-type GaSb, indicating the formation of crystalline GaSb (Fig. 9). The lattice parameter was determined as 608(2) pm, which agrees very well with the literature value of 609.5 pm.[23]

Electron diffraction patterns of a single needle show single Bragg intensities of cubic GaSb. In diffraction patterns along the [011]-type zone axis additional reflections in the *h*-direction could be observed. These additional intensities are caused by {111}-type mirror twins. They are also present in diffractograms (FFT's) of high resolution TEM (HR-TEM) images of the same direction.

HR-TEM lattice images were taken perpendicular to the long axis of the needle. Only the edge of the needle is sufficiently electron transparent, while it grows stepwise thicker

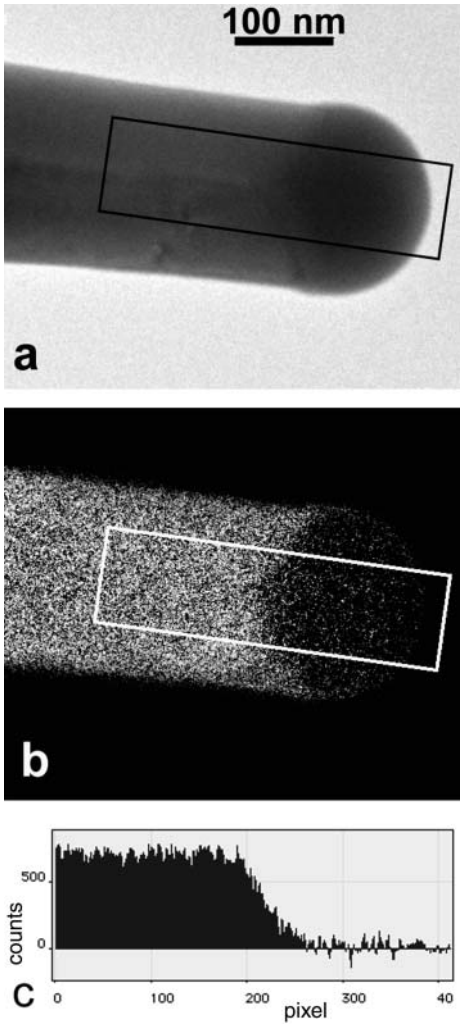

Fig. 7 TEM bright-field image of the tip of a single needle (a) and Sb-distribution map of the same region (b). Part (c) shows the profile of the Sb distribution taken from the marked box in (a) and (b).

towards the middle. The measured distances of the lattice planes agree well with the *d*-spacings of cubic GaSb. The marked distances in Fig. 10a, recorded along the [110] zone axis, correspond to 10 lattice spacings of the type {200} ($d=3.04$ nm) and {220} ($d=2.14$ nm) and those in Fig. 10b, recorded along the [112] zone axis, to 10 lattice spacings of the type {111} ($d=3.49$ nm) and {220} ($d=2.14$ nm), respectively. In addition, the small oxygen-containing amorphous border can clearly be observed. Beside large areas free of defects, some stacking faults and twin boundaries are found in the lattice images, especially along the [110]-type zone axis.

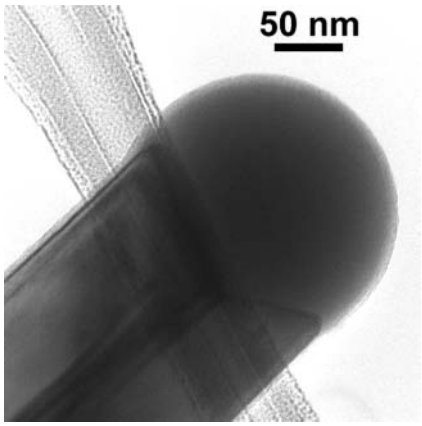

Fig. 8 TEM bright-field image of a GaSb needle showing the twinning.

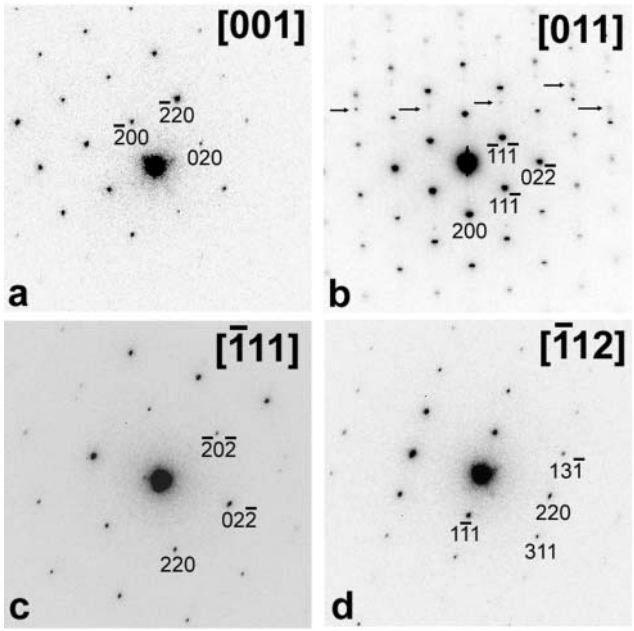

Fig. 9 Selected area electron diffraction patterns of a single, crystalline GaSb needle taken at different orientations. ED pattern (b), taken along the [011] zone axis, shows additional intensities (arrows), caused by {111}-type twins.

Whisker growth mechanism

The growth of the dendritic-type crystals depends on the temperature conditions as was demonstrated by pyrolysis at different temperatures. Fig. 11 shows typical SEM images of samples obtained at 275 °C and 450 °C.

At 275 °C, no dendrites but only single GaSb needles of 2–5 μm in length were formed. In contrast, the film obtained at

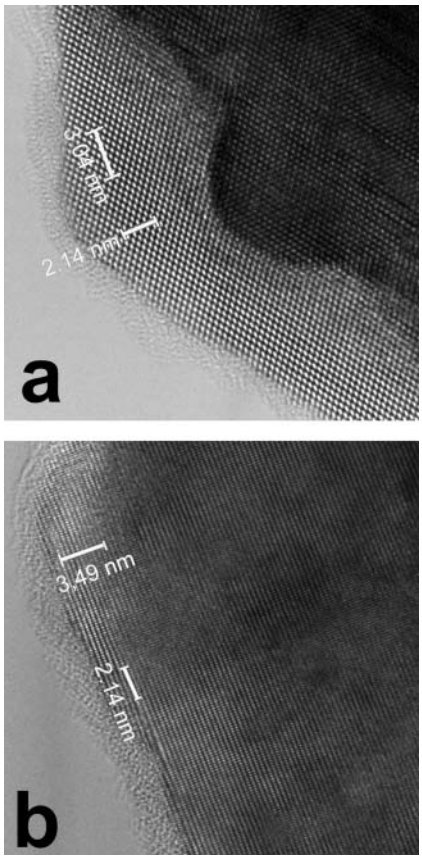

Fig. 10 HR-TEM lattice images of a GaSb needle taken along the [110]- (a) and [112]-type zone axes (b), respectively.

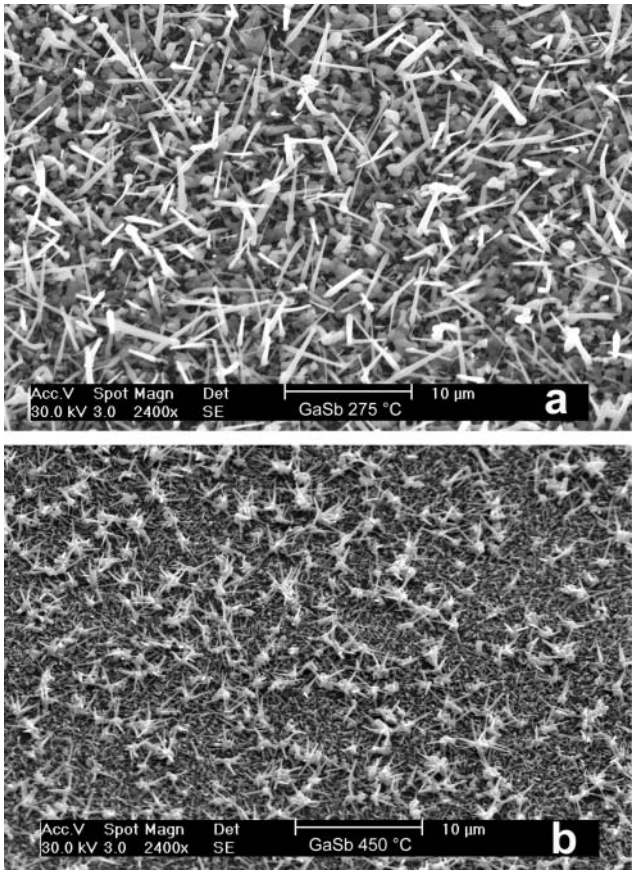

Fig. 11 Typical SEM images of GaSb samples obtained from **2** at 275 °C and 450 °C.

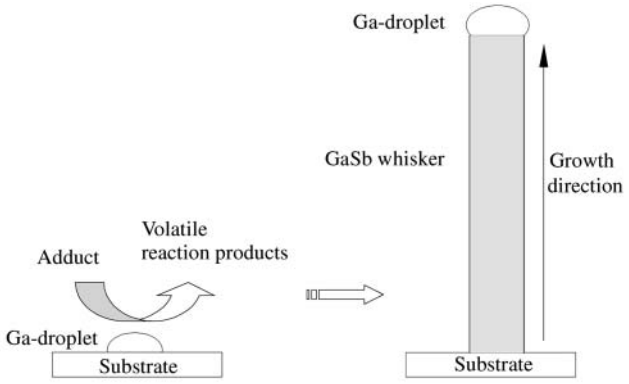

Fig. 12 Scheme of the VLS whisker growth mechanism.

450 °C shows a significantly denser dentrite coverage compared to the film obtained at 400 °C. Again, both the single needles and the dendrites are crystalline, pure GaSb and both show Ga spherules at their tips. However, while those of the sample obtained at 450 °C contain only amorphous Ga (Sb < 1%), the Sb concentration of the tips at single needles obtained at 275 °C is higher (4–5%). Sb is present in the form of crystalline GaSb in the spherules, as was demonstrated by electron diffraction studies. Obviously, both the Sb concentration and the crystallinity of the GaSb within the tips depend on the pyrolysis temperature.

The single needles and the needles of the dendrites are known as *whiskers*. It is well established that whiskers can be formed from the gas phase by thermolysis of molecular precursors and their synthesis was investigated intensively due to their fascinating physical properties.[24] Most of the studies have concentrated on the synthesis of technologically important Al_2O_3, Si, SiC or Si_3N_4 whiskers, which are powerful additives for ceramic materials, improving their mechanical strength dramatically.[25] Besides this class, whiskers containing group 13–15 elements were also synthesized, *e.g.* AlN, GaN, GaAs and InP.[26] The whisker growth process is fully understood since the seminal work of Ellis and Wagner.[27] The most important growth mechanism is the so-called VLS process (*vapor–liquid–solid*) (Fig. 12). At the interface between a liquid phase, usually a metal with a low melting point, and the gas phase thermally induced decomposition reactions of the precursors occur. The small liquid droplets, *e.g.* elemental Au, are usually generated by sputtering, laser ablation or chemical vapor deposition before the decomposition reaction of the precursors.[28] However, they can also be formed during the decomposition process when two or more precursors with different decomposition temperatures are used, which is likely in CVD reactions. The droplets serve both as a catalyst for the decomposition of the precursors, reducing the decomposition temperature significantly, and as a solvent for the decomposition products (elements). After becoming supersaturated in the droplet, precipitation starts, leading to the growth of a single crystal at the interface between the liquid and the solid phase (substrate). The droplet typically remains at the tip of the whisker.[29] A comparable mechanism is true for the SLS process (*solution–liquid–solid*), which was introduced by Buhro *et al.*.[30] In contrast to the VLS process, the whiskers are grown in solution. However, the growth mechanism is almost the same. The SLS process also occurs in the presence of a metallic liquid droplet, which initializes the whisker growth. As was found for the VLS process, the droplet remains at the tip of the resulting whisker.

In our case, the initializing Ga droplet is formed *in situ* by thermal decomposition of *t*-Bu_3Ga, which probably is present in the gas phase due to some dissociation of the starting adduct. Further decomposition reactions of the tri-*tert*-butylgallane and the triisopropylstibine occur preferentially at the Ga droplets. The resulting elemental Ga and Sb dissolve in the droplet, until the solution supersaturates with Sb and the growth of crystalline GaSb whiskers occurs at the liquid–solid interface. However, our results clearly show a temperature dependence of the whisker growth, which may be explained as follows. At low temperatures, the decomposition rate of the stibine is low. This leads to a slow enrichment with Sb and local inhomogeneities of the Sb concentration in the Ga droplet are avoided. Therefore, the precipitation of the GaSb whisker takes place in a controlled manner, when the supersaturation is reached, leading to the formation of single GaSb needles.

In contrast, high temperatures yield high decomposition rates, which favor the formation of inhomogeneities of Sb within the molten Ga droplet. Therefore, local supersaturation within the droplet is possible, resulting in simultaneous, uncontrolled growth of several needles from a single droplet. Consequently, dendritic-shaped crystals are formed.[31]

The formation of GaSb whiskers needs temperatures of at least 275 °C, while at lower temperatures (250 °C) the decomposition of the precursor is incomplete.[32] However, these temperature are much below the temperatures typically needed for the deposition of GaSb thin films by CVD processes, which usually range from 500 to 550 °C. Obviously, the Ga droplets catalyse the decomposition of the trialkylgallane and stibine. Analogous results were reported for the synthesis of Si whiskers. By using small Au droplets deposited on a Si substrate, the reaction temperature was lowered from 1400 °C (on a pure Si substrate) to 700 °C. At the same time the growth rate increases significantly (20 times higher). With Pt droplets, the results were even more impressive, since the growth rate became 60 times higher.

In case of III–V materials, whisker growth was realized for nitrides, phosphides and arsenides while to the best of our knowledge, Sb-containing whiskers haven't been grown, so far. The temperatures which are necessary for the growth of III–V

whiskers are material-specific. While AlN whiskers were obtained at temperatures above 1000 °C,[33] GaN whiskers were grown at 910 °C[25g] and GaAs whiskers were grown from Ga/$AsCl_3$/H_2 and $GaCl_3$/$AsCl_3$/H_2 on quartz glass or GaAs substrates, which were covered with small Ga droplets, between 550 and 680 °C.[34] Compared to these temperatures, the temperatures necessary for the growth of GaSb whiskers as reported herein are very low. Currently we are investigating the growth of GaSb whiskers in detail in the gas phase and in solution.

Summary and conclusion

Pure GaSb crystals were obtained by thermal decomposition of two different single source precursors in sealed glass tubes in the temperature range between 250 and 450 °C. Dependent on the precursor and the reaction temperature, simple GaSb crystallites as well as GaSb dendrites and single GaSb needles were obtained. The crystallites were characterized by means of EM methods such as SEM, TEM, EDX, EELS, and electron diffraction studies. Common crystal sizes vary from 500 to 1000 nm, while the needles are up to 5 μm in length. Carbon couldn't be detected in any sample, while O is present due to some surface oxidation. In particular the absence of any C within the particles as well as the low decomposition temperatures observed for almost complete pyrolysis of the precursors demonstrate the single source concept to be promising for the synthesis of the desired class of materials. The specific adducts used in these preliminary studies seem to be suitable candidates to serve as single source precursors for the growth of thin GaSb films by the MOCVD process. Results on detailed studies will be reported in the future.

Acknowledgements

Stephan Schulz gratefully acknowledges the financial support by the BMBF, the Fonds der Chemischen Industrie, the DFG and Prof. E. Niecke, Universität Bonn. In addition, the authors would like to thank Prof. W. Mader, Universität Bonn, for his kind cooperation.

References

1 A. Y. Polyakov, M. Stam, A. G. Milnes, R. G. Wilson, Z. Q. Fang, P. Rai-Choudhury and R. J. Hillard, *J. Appl. Phys.*, 1992, **72**, 131.
2 C. R. Bolognesi, E. J. Caine and H. Kroemer, *IEEE Electron Device Lett.*, 1994, **EDL-15**, 16.
3 (*a*) L. Samoska, B. Brar and H. Kroemer, *Appl. Phys. Lett.*, 1993, **62**, 2539; (*b*) Y. Zhang, N. Baruch and W. I. Wang, *Appl. Phys. Lett.*, 1993, **63**, 1068; (*c*) H. K. Choi and G. W. Turner, *Appl. Phys. Lett.*, 1995, **67**, 332; (*d*) Y.-H. Zhang, *Appl. Phys. Lett.*, 1995, **66**, 118.
4 (*a*) A. F. J. Levi and T. H. Chiu, *Appl. Phys. Lett.*, 1987, **51**, 984; (*b*) H. Lee, P. K. York, R. J. Menna, R. U. Martinelli, D. Z. Garbuzov, S. Y. Narayan and J. C. Connolly, *Appl. Phys. Lett.*, 1995, **66**, 1942.
5 (*a*) H. K. Choi, G. W. Turner and Z. L. Liau, *Appl. Phys. Lett.*, 1994, **65**, 2251; (*b*) J. Schmitz, J. Wagner, F. Fuchs, N. Herres, P. Koidl and J. D. Ralston, *J. Cryst. Growth*, 1995, **150**, 858; (*c*) M. Yano, K. Yamamoto, T. Utatsu and M. Inoue, *J. Vac. Sci. Technol. B*, 1994, **12**, 1133.
6 A. N. Baranov, C. Fouillant, P. Grunberg, J. L. Lazzari, S. Gaillard and A. Jouille, *Appl. Phys. Lett.*, 1994, **65**, 616.
7 H. Manasevit, *Appl. Phys. Lett.*, 1968, **12**, 156.
8 For an excellent review see the following and the references cited therein: A. Aardvark, N. J. Mason and P. J. Walker, *Prog. Cryst. Growth Charact.*, 1997, **35**, 207.
9 See for example: (*a*) A. Subekti, E. M. Goldys, M. J. Paterson, K. Drozdowics-Tomsia and T. L. Tansley, *J. Mater. Res.*, 1999, **14**, 1238; (*b*) E. Alphandéry, R. J. Nicholas, N. J. Mason, B. Zhang, P. Möck and G. R. Booker, *Appl. Phys. Lett.*, 1999, **74**, 2041; (*c*) S. S. Yi, D. M. Hansen, C. K. Inoki, D. L. Harris, T. S. Kuan and T. F. Kuech, *Appl. Phys. Lett.*, 2000, **77**, 842; (*d*) L. Müller-Kirsch, U. W. Pohl, R. Heitz, H. Kirmse, W. Neumann and D. Bimberg, *J. Cryst. Growth*, 2000, **221**, 611; (*e*) S. S. Yi, P. D. Moran, X. Zhang, F. Cerrina, J. Carter, H. I. Smith and T. F. Kuech, *Appl. Phys. Lett.*, 2001, **78**, 1358.
10 Very recently, the growth of AlSb films using various alane precursors by the MOCVD process in a multiwafer planetory reactor has been studied in detail. C. Agert, P. Lanyi and A. W. Bett, *J. Cryst. Growth*, 2001, **225**, 426.
11 (*a*) M. A. Todd, G. Bandari and T. H. Baum, *Chem. Mater.*, 1999, **11**, 547; (*b*) B. C. Harrison and E. H. Tompkins, *Inorg. Chem.*, 1962, **1**, 951; (*c*) O. Sugiura, H. Kameda, K. Shiina and M. Matsumura, *J. Electron. Mater.*, 1988, **17**, 11.
12 (*a*) G. T. Stauff, D. K. Gaskill, N. Bottka and R. W. Gedridge Jr., *Appl. Phys. Lett.*, 1991, **58**, 1311; (*b*) C. H. Chen, G. B. Stringfellow, D. C. Gordon, D. W. Brown and B. A. Vaartstra, *Appl. Phys. Lett.*, 1992, **61**, 204; (*c*) R. M. Grahem, A. C. Jones, N. J. Mason, S. A. Rushworth, L. Smith and P. J. Walker, *J. Cryst. Growth*, 1994, **145**, 363; (*d*) C. H. Chen, C. T. Chiu, C. B. Stringfellow and R. W. Gedridge Jr., *J. Cryst. Growth*, 1992, **124**, 88; (*e*) R. M. Biefeld, A. A. Allerman and S. R. Kurtz, *J. Cryst. Growth*, 1997, **174**, 593; (*f*) D. S. Cao, Z. M. Fang and G. B. Stringfellow, *J. Cryst. Growth*, 1991, **113**, 441; (*g*) C. W. Wang, M. C. Finn, S. Salim, K. F. Jensen and A. C. Jones, *Appl. Phys. Lett.*, 1995, **67**, 1384; (*h*) C. W. Wang, K. F. Jensen, A. C. Jones and H. K. Choi, *Appl. Phys. Lett.*, 1996, **68**, 400; (*i*) R. M. Biefeld, A. A. Allerman and M. W. Pelczynski, *Appl. Phys. Lett.*, 1996, **68**, 932.
13 J. Shin, A. Verma, G. B. Stringfellow and R. W. Gedridge, *J. Cryst. Growth*, 1994, **143**, 15.
14 (*a*) A. H. Cowley, R. A. Jones, C. M. Nunn and D. L. Westmoreland, *Chem. Mater.*, 1990, **2**, 221; (*b*) H. S. Park, S. Schulz, H. Wessel and H. W. Roesky, *Chem. Vap. Deposit.*, 1999, **5**, 179.
15 (*a*) L. M. Nemirowskii, B. I. Kozyrkin, A. F. Lanstov, B. G. Gribov, I. M. Skvortsov and I. A. Sredinskaya, *Dokl. Akad. Nauk SSSR*, 1974, **214**, 590; (*b*) A. H. Cowley, R. A. Jones, K. B. Kidd, C. M. Nunn and D. L. Westmoreland, *J. Organomet. Chem.*, 1988, **341**, C1; (*c*) A. R. Barron, A. H. Cowley, R. A. Jones, C. M. Nunn and D. L. Westmoreland, *Polyhedron*, 1988, **7**, 77; (*d*) S. Schulz, T. Schoop, H. W. Roesky, L. Häming, A. Steiner and R. Herbst-Irmer, *Angew. Chem., Int. Ed. Engl.*, 1995, **34**, 919.
16 (*a*) S. Schulz and M. Nieger, *J. Organomet. Chem.*, 1998, **570**, 275; (*b*) S. Schulz and M. Nieger, *J. Chem. Soc., Dalton Trans.*, 2000, 639; (*c*) S. Schulz and M. Nieger, *Organometallics*, 1998, **17**, 3398; (*d*) S. Schulz and M. Nieger, *Organometallics*, 1999, **18**, 315; (*e*) S. Schulz and M. Nieger, *Organometallics*, 2000, **19**, 699; (*f*) S. Schulz, A. Kuczkowski and M. Nieger, *J. Organomet. Chem.*, 2000, **604**, 202; (*g*) S. Schulz and M. Nieger, *Organometallics*, 2000, **19**, 2640.
17 (*a*) R. A. Baldwin, E. E. Foos, R. L. Wells, P. S. White, A. L. Rheingold and G. P. A. Yap, *Organometallics*, 1996, **15**, 5035; (*b*) R. L. Wells, E. E. Foos, P. S. White, A. L. Rheingold and L. M. Liable-Sands, *Organometallics*, 1997, **16**, 4771; (*c*) E. E. Foos, R. J. Jouet, R. L. Wells, A. L. Rheingold and L. M. Liable-Sands, *J. Organomet. Chem.*, 1999, **582**, 45; (*d*) E. E. Foos, R. L. Wells and A. L. Rheingold, *J. Cluster Sci.*, 1999, **10**, 121; (*e*) H. J. Breunig, M. Stanciu, R. Rösler and E. Lork, *Z. Anorg. Allg. Chem.*, 1998, **624**, 1965.
18 The bond strength of metal–carbon bonds generally decrease with increasing chain length and/or steric branching. This can be demonstrated by DSC experiments, which show a decrease of the decomposition temperature. This decreasing stability is based on both the increase of the radical stability with increased steric branching and on the facile β-H elimination of alkene from higher alkyl compounds. Therefore, the Sb–carbon bond strengths for several triorganostibines decrease in the following order: Me_3Sb (233.9 kJ mol^{-1}) > $(vinyl)_3Sb$ (205 kJ mol^{-1}) > *i*-Pr_3Sb (126.8 kJ mol^{-1}) > $(allyl)_3Sb$ (90.4 kJ mol^{-1}): A. C. Jones and P. O'Brien, in *CVD of Compound Semiconductors*, VCH, Weinheim, 1997, p. 146. Slightly different values are given in *Handbook of Chemistry and Physics*, 78th edn., ed. D. R. Lide, CRC Press, New York, 1997, pp. 9–67: Me_3Sb (255 ± 17 kJ mol^{-1}) > Et_3Sb (243 ± 17 kJ mol^{-1}).
19 The spectra were quantified using the Sb-L and Ga-K lines with calculated weight-percentages of 36.41 and 63.59 for Ga and Sb in GaSb.
20 The quantification of EEL spectra uses the intensity of ionization edges in a energy interval of 10 to 200 eV after the edge. In the given situation with a narrow O K-edge and with the Sb M-edge present in the same spectrum, only the counts from a 5 eV energy interval can be used, leading to large standard deviations for the

results. Oxygen was determined to be present with an amount of $\sim 1\%$ within thin areas of the samples.
21 These studies won't be discussed in detail here since they are very similar to those of precursor **1**.
22 The calculation of the elemental map was performed using the so-called three windows method. Three energy filtered images were recorded at different ranges of energy loss, two images with energy losses in front of the ionization edge (pre edge 1: $\Delta E = 490 \pm 20$ eV; pre edge 2: $\Delta E = 520 \pm 20$ eV) and one image on the ionization edge (post edge:$\Delta E = 552 \pm 20$ eV), using a slit aperture of 20 eV in the energy dispersive plane of the filter. All pictures were cross-correlated to correct for unavoidable image drift. The images in front of the edge were used for the pixel by pixel calculation of the background intensity of the post edge image. The result after background subtraction is a elemental distribution map.
23 GaSb, space group $F\bar{4}3m$, $a = 609.5$ pm; *Natl. Bur. Stand. (U.S.)*, Circ. 539 6 30, 1956. JCPDF-Card P070215.
24 See for example: C. C. Evans, in *Whiskers*, Mills & Boon Limited, London, 1972, pp. 33ff.
25 H. Y. Peng, X. T. Zhou, H. L. Lai, N. Wang and S. T. Lee, *J. Mater. Res.*, 2000, **15**, 2020.
26 (*a*) R. L. Barns and W. C. Ellis, *J. Appl. Phys.*, 1965, **36**, 2296; (*b*) C. M. Wolfe, C. J. Nuese and N. Holonyak Jr., *J. Appl. Phys.*, 1965, **36**, 3790; (*c*) W. C. Ellis, C. J. Frosch and R. B. Zetterstrom, *J. Cryst. Growth*, 1968, **2**, 61; (*d*) J. J. Nickl and W. Just, *J. Cryst. Growth*, 1971, **11**, 11; (*e*) M. Yazawa, M. Koguchi and K. Hiruma, *Appl. Phys. Lett.*, 1991, **58**, 1080; (*f*) M. Yazawa, M. Koguchi, A. Muto and K. Hiruma, *Adv. Mater.*, 1993, **5**, 577; (*g*) C.-C. Chen, C.-C. Yeh, C.-H. Chen, M.-Y. Yu, H.-L. Liu, J.-J. Wu, K.-H. Chen, L.-C. Chen, J.-Y. Peng and Y.-F. Chen, *J. Am. Chem. Soc.*, 2001, **123**, 2791; (*h*) P. D. Markowitz, M. P. Zach, P. C. Gibbons, R. M. Penner and W. E. Buhro, *J. Am. Chem. Soc.*, 2001, **123**, 4502.
27 R. S. Wagner and W. C. Ellis, *Appl. Phys. Lett.*, 1964, **4**, 89.
28 See for example: (*a*) X. Duan and C. M. Lieber, *Adv. Mater.*, 2000, **12**, 298; (*b*) C.-C. Chen and C.-C. Yeh, *Adv. Mater.*, 2000, **12**, 738; (*c*) J. A. Haber, P. C. Gibbons and W. E. Buhro, *Chem. Mater.*, 1998, **10**, 4062; (*d*) K. Haraguchi, K. Hiruma, K. Hosomi, M. Shirai and T. Katsuyama, *J. Vac. Sci. Technol. B*, 1997, **15**, 1685.
29 Very recently, the VLS mechanism was confirmed at the nanometer scale by direct, *in-situ* observation of nano-wire growth in a transmission electron microscope at high temperatures. Y. Wu and P. Yang, *J. Am. Chem. Soc.*, 2001, **123**, 3165.
30 T. J. Trentler, K. M. Hickman, S. C. Goel, A. M. Viano, P. C. Gibbons and W. E. Buhro, *Science*, 1995, **270**, 1791.
31 See also for example: C. C. Evans, in *Whiskers*, Mills & Boon Limited, London, 1972, p. 45.
32 The glass tube is covered after pyrolysis at 250 °C with an almost colorless, crystalline film which contains large amounts of the starting adduct, as was shown by NMR studies. Obviously, only sublimation occurred.
33 J. A. Haber, P. C. Gibbons and W. E. Buhro, *J. Am. Chem. Soc.*, 1997, **119**, 5455.
34 W. Just, J. J. Nickl and H.-J. Kaiser, *Angew. Chem., Int. Ed. Engl.*, 1971, **10**, 847.